JOURNAL OF GEOPHYSICAL RESEARCH, VOL. 106, NO. A12, PAGES 29,531–29,542, DECEMBER 1, 2001

Computational analysis of the near-Earth magnetospheric current system during two-phase decay storms

M. W. Liemohn, J. U. Kozyra, C. R. Clauer, and A. J. Ridley

Space Physics Research Laboratory, University of Michigan, Ann Arbor, Michigan, USA

Abstract. Several two-phase decay magnetic storms are examined using a kinetic transport model to find the spatial and temporal distribution of the perpendicular and field-aligned currents in the inner magnetosphere. The global morphology of these currents in the calculational domain (inside of geosynchronous orbit) is discussed as a function of storm epoch, obtaining good comparison between the numerically derived features and observed values of stormtime currents in this region. The model results are also consistent with quiet time plasma observations showing an increasing pressure in to L=3 or 4, including a pressure maximum near midnight for the generation of region 2 Birkeland currents in the proper direction. A detailed analysis of the characteristic features of these currents is also presented and discussed. It is found that most of the ring current (>90%) during the main phase and early recovery phase is partial rather than symmetric, closing mostly (up to 90%) through field-aligned currents into the ionosphere. Conversely, the quiet time ring current is largely (>60%) symmetric, with most of the asymmetry produced by minor injections of near-Earth plasma sheet material. In general, the peak asymmetric current (which occurs during the main phase) is 2-3 times larger than the peak symmetric current (which occurs during the recovery phase) for any particular two-phase decay event. This is the case for all of the events studied, regardless of storm size, solar wind parameters, or solar cycle. The maximum azimuthal current (integrated over a local time slice) reaches 5 to 20 MA, compared with <2 MA of symmetric current at quiet times.

1. Introduction

Recent investigations of ring current dynamics are leading to a new understanding of the stormtime ring current during events with two-phase decay signatures. It has been thought that a trapped symmetric ring current is rapidly produced after the *Dst* minimum during storms. The subsequent ring current decay was thought to be dominated by charge exchange, with minor contributions from Coulomb drag energy loss and wave-particle scattering into the loss cone (see most recent review by *Daglis et al.* [1999]). Two-phase decays were thought to be produced by the different charge exchange rates of O^+ and H^+ ring current ions, particularly for large storms [e.g., *Hamilton et al.*, 1988]. It is now clear that the partial ring current far exceeds the symmetric ring current not only throughout the entire main phase of magnetic storms (which typically last from several hours to more than a day) but also throughout the early recovery phase of two-phase decay storms [*Terada et al.*, 1998; *Ebihara and Ejiri*, 1998; *Grafe*, 1999; *Liemohn et al.*, 1999, 2001; *Greenspan and Hamilton*, 2000; J. U. Kozyra et al., Multistep *Dst* development and ring current composition changes during the June 4-6, 1991, magnetic storm, submitted Journal of Geophysical Research, 2001 (hereinafter referred to as (Kozyra et al., submitted manuscript, 2001)]. A large enhancement in the convection electric field and near-Earth plasma sheet density are the major drivers of the ring current development, with the field transporting the particles deep into the inner magnetosphere. During the main phase, plasma sheet ions drift around the duskside and then flow out the dayside magnetopause, with most of them making a single pass by the Earth. When the convection electric field decreases (late in the recovery phase), open drift paths are converted to closed ones, finally forming a symmetric ring current. By this time, much of the energy contained in the ring current (partial and symmetric) has already been dissipated [*Liemohn et al.*, 2001].

An understanding of the morphology and evolution of the current in the inner magnetosphere is needed for several reasons. First, the magnetic field perturbations generated by these currents alter the magnetic field in this region [e.g., *Chun and Russell*, 1997], having consequences for all of the plasma populations, especially the high-energy radiation belt particles. Second, the ionospheric closure of the asymmetric portion of these currents leads to large perpendicular electric fields at subauroral latitudes during disturbances, having significant effects on ionospheric plasma drifts [e.g., *Fejer et al.*, 1990; *Yeh et al.*, 1991]. These drifts cause density irregularities that cause VHF scintillations and therefore GPS (global positioning system) errors. Third, these currents are part of the overall magnetospheric current system and should be understood in relation to other magnetospheric currents, particularly the region 1 Birkeland currents and Chapman-Ferraro magnetopause currents.

In situ observations yield two products for understanding the current system in the inner magnetosphere. The first is single-point measurements of the current density at a particular location and time. These are useful for understanding the local current intensity as a function of the solar wind and planetary conditions, but they do not resolve space-time ambiguities. The second is statistical compilations of these

Paper number 2001JA000045.
0148-0227/01/2001JA000045$09.00

measuremets as functions of various quantities. These are useful for understanding general trends in the global morphology and evolution of the current system, but they cannot predict the extreme events or even precisely reproduce the global pattern for any particular event.

Theoretical calculations have the power to determine the current everywhere in near-Earth space for a specific event. However, very few numerical studies of the stormtime ring current actually calculate and present the magnetospheric current densities. For instance, the field-aligned currents from the magnetospheric particle populations have been numerically calculated as part of the Rice Convection Model (RCM) for several decades [e.g., *Jaggi and Wolf*, 1973; *Harel et al.*, 1981; *Spiro et al.*, 1988]. From these currents the RCM has been used quite successfully to reproduce ionospheric electric field observations [*Spiro et al.*, 1988; *Fejer et al.*, 1990; *Fejer and Scherliess*, 1997; *Garner*, 2000]. However, discussion of the calculated region 2 Birkeland currents is usually brief with no presentation of the magnetospheric cross-field currents generating them. For example, *Chen et al.* [1982] certainly calculated the magnetospheric currents from the RCM to obtain synthetic ground-based magnetograms, but no presentation or discussion of their morphology and evolution is given.

More recent numerical investigations are similarly vague about the inner magnetospheric current. *Takahashi et al.* [1991] calculated the current densities in the ring current region, but only presented the field-aligned currents into the ionosphere, which unfortunately gave unreasonably large ionospheric currents and magnetic perturbations. Only very recently has the stormtime perpendicular current density in the inner magnetosphere been calculated and presented from numerical simulation results of geomagnetic storms [*Ebihara and Ejiri*, 2000; Kozyra et al., submitted manuscript, 2001]. Both of these studies showed that the azimuthal current in the inner magnetosphere is asymmetric during storm main phases, but did not analyze these values any further than topological discussions.

This study quantitatively examines the three-dimensional current distribution in the inner magnetosphere by analyzing numerical results for several geomagnetic storms. Both cross-field and field-aligned currents are considered as a function of storm epoch, including an analysis of the proportion of the asymmetric ring current closing through various places. These calculated values are compared against observations and put into the context of previous studies.

2. Approach

This study uses results from a kinetic ring current model that solves the gyration and bounce-averaged Boltzmann equation inside of geosynchronous orbit. Originally developed by *Fok et al.* [1993] and *Jordanova et al.* [1996], the version used here is most recently described by *Liemohn et al.* [1999, 2001]. Using second-order accurate numerical schemes, the hot ion phase-space distribution is determined as a function of time, equatorial plane location, energy, and equatorial pitch angle, yielding a detailed description of the ring current ion population throughout near-Earth space. Using solar wind data, geomagnetic activity indices, and geosynchronous orbit plasma data, quantitative results are found for specific magnetic storm events. For the calculations presented below it should be noted that the geomagnetic field is taken to be a static dipole and the convection electric field is specified by a modified *McIlwain* [1986] description. The particular realization used here has the field driven by the cross polar cap potential difference (as given by the assimilative mapping of ionospheric electrodynamics (AMIE) technique) and also by the midnight auroral boundary index (MBI) produced by the Air Force Research Laboratory (see *Liemohn et al.* [2001] for further details).

The ion distributions can be integrated to yield the current density $\mathbf{J}$ in the inner magnetosphere. First, $\mathbf{J}$ must be calculated from the ring current results for the entire simulation domain. The perpendicular current from the hot ion population of the inner magnetosphere can be written as the sum of two terms which drive the electrons and ions in opposite directions [e.g., *Parker*, 1957], the first being the magnetization current driven by the cyclotron motion,

$$\mathbf{J}_{\perp,M}=-\nabla\times\left(\frac{P_\perp\mathbf{B}}{B^2}\right)=\frac{\mathbf{B}}{B^2}\times\left[\nabla P_\perp-P_\perp\frac{\nabla B}{B}-P_\perp\frac{(\mathbf{B}\cdot\nabla)\mathbf{B}}{B^2}\right], \quad (1)$$

and the second being the current from the drifts induced by the gradient and curvature of the ambient magnetic field $\mathbf{B}$,

$$\mathbf{J}_{\perp,GC}=+\frac{\mathbf{B}}{B^2}\times\left[P_\perp\frac{\nabla B}{B}+P_{||}\frac{(\mathbf{B}\cdot\nabla)\mathbf{B}}{B^2}\right]. \quad (2)$$

Note that (1) and (2) are written for ion pressures because these particles carry the majority of the plasma energy. Using some well-known vector identities and the assumption of a potential magnetic field (that is, a current-free representation, such as a dipole, which is used in the transport model), (1) and (2) can be summed and rewritten as [cf. *Lui et al.*, 1987; *Ebihara and Ejiri*, 1998]

$$\mathbf{J}_\perp=\frac{\mathbf{B}}{B^2}\times\left[\nabla P_\perp+\left(P_{||}-P_\perp\right)\frac{\nabla B}{B}\right]. \quad (3)$$

Note that there is both a radial and azimuthal component to $\mathbf{J}_\perp$. The particle pressures in (3) are simply moments of the calculated distribution function,

$$\begin{aligned} P_\perp &= \pi\int f(v,\alpha)mv^2\sin^3\alpha dv d\alpha\,, \\ P_{||} &= 2\pi\int f(v,\alpha)mv^2\cos^2\alpha\sin\alpha dv d\alpha\,, \end{aligned} \quad (4)$$

where v and α are the particle velocity and local pitch angle and f is found by mapping the distribution at the equatorial plane (the bounce-averaged value) to the local latitude. The current in (3) was used in the Biot-Savart law and analytically integrated to yield a relationship between the total ring current energy and its resulting magnetic perturbation at the center of the Earth, known as the Dessler-Parker-Sckopke (DPS) equation [*Dessler and Parker*, 1959; *Sckopke*, 1966].

The current density parallel to the magnetic field lines is found from the divergence of $\mathbf{I}_\perp$ (current, not current density) according to Kirchhoff's branch point rule,

$$\mathbf{B}\cdot\nabla\left(\frac{J_{||}}{B}\right)=\nabla\cdot\mathbf{J}_\perp\,, \quad (5)$$

which is accumulated along the field line,

$$J_{||}(\mathbf{r}')=\frac{1}{A_{||}(\mathbf{r}')}\sum_{k=k_{eq}}^{k(\mathbf{r}')}\left[\sum_{i=\perp\text{ faces}}A_{i,k}(k)\mathbf{J}_{\perp,i,k}(k)\cdot\hat{\mathbf{n}}_{i,k}(k)\right], \quad (6)$$

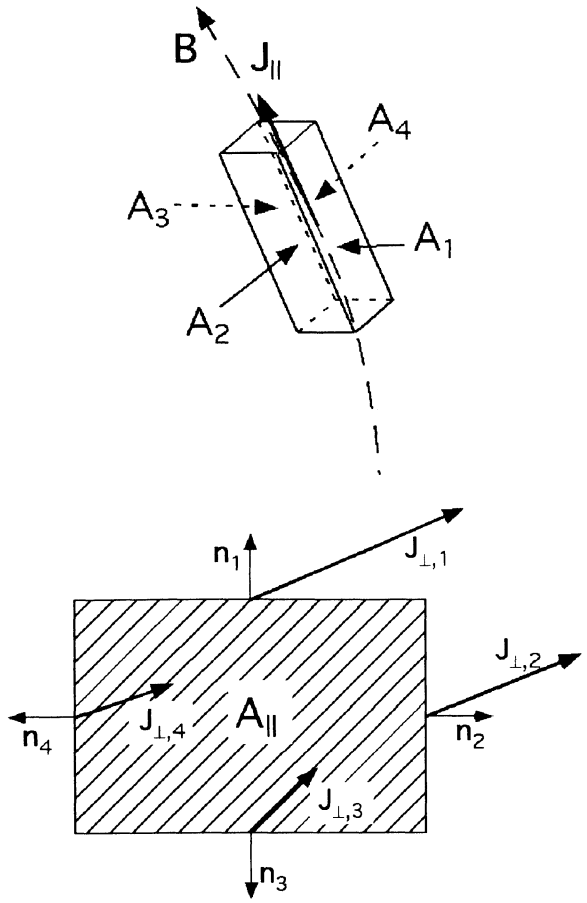

Figure 1. Schematic of the geometry for the calculation of the parallel current density, showing a three-dimensional view of a grid cell along a field line and a cross-sectional view that cell.

where $A_{\|}$ is the cross-sectional area of the local grid cell, k is the grid cell index along the field line, $A_{i,k}$ is the surface area between cell k and adjacent cells normal to $\mathbf{B}_k$ (in the direction $\mathbf{n}_{i,k}$), and $\mathbf{J}_{\perp i,k}$ is the current at that cell interface. The outer summation runs from the equatorial plane to the local cell along $\mathbf{B}$, and the inner summation includes all perpendicular interface surfaces for the chosen cell. This is schematically shown in Figure 1 for an arbitrary grid cell. Note that the grid cells are actually curved with the spatial grid. Equation (6) is equivalent to the Vasyliunas equation for the current into the ionosphere [*Vasyliunas*, 1970],

$$J_{\|,iono}=\frac{B_{iono}}{2B_{eq}^2}\left(\nabla P_{eq}\times\mathbf{B}_{eq}\right)\cdot\nabla_{eq}\left(\int\frac{dl}{B}\right), \qquad (7)$$

given an isotropic pressure (the subscripts *iono* and *eq* refer to the ionosphere and equatorial plane, respectively). *Birmingham* [1992] extended the Vasyliunas equation by deriving a formulation for the field-aligned current accumulation between two arbitrary points along a field line, including pressure anisotropy effects. However, the grid-based, numerical nature of the model results makes (6) a more convenient expression for the field-aligned current densities than either (7) or Birmingham's integral equation.

The field-aligned current (FAC) deposited into or extracted from the ionosphere is then somehow closed through Pedersen currents, either with itself or through the region 1 current system. The nature of this ionospheric portion of the closure current will not be discussed here, as the focus is on the magnitudes of the currents in the inner magnetosphere.

3. Results

For this analysis, simulation results for four magnetic storms will be examined: September 25, 1998; June 5, 1991; May 15, 1997; and October 19, 1998. All of these storms are driven by interplanetary coronal mass ejections (ICMEs), and all have varying degrees of a two-phase decay recovery. The first will be shown in detail and summary plots of the rest will be used to demonstrate the generality of the conclusions. For details on the various input quantities and other simulation results, please see Kozyra et al. (submitted manuscript, 2001) for the June 1991 storm and *Liemohn et al.* [2001] for the others. The model accurately reproduced the observed features of the ion distributions and *Dst** for these storms (see figures below), and these results helped to solidify the new understanding of the stormtime ring current. Here another aspect of these results will be investigated: the magnitude, morphology, and evolution of the current itself and not just the particle populations.

3.1. Global Morphology

Plate 1 shows several quantities in dial plot format at seven times during the September 1998 event. The chosen times (from left to right) are during the storm growth phase (first two columns), the modeled *Dst** minimum (third column), the early recovery phase (fourth column), the transition between early and late recovery (fifth column), and the late recovery phase (last two columns). The top row shows the flux tube-averaged pressure of the ring current ions (summed H^+ and O^+). The ions stream in from the nightside (the right in each dial plot), drift around the duskside (the bottom of each dial plot), and convect out the dayside boundary. The particles flush out the dayside throughout the main phase and early recovery [cf., *Liemohn et al.*, 1999, 2001], and it is not until convection has significantly decreased that the ring current energy density appears symmetric.

According to (3), $\mathbf{J}_{\perp}$ should flow along the surfaces of constant pressure, slightly deviated from these isobars by the anisotropy term (in general less than the pressure gradient term, as will be shown below). This is what is seen in the next two rows of Plate 1, showing the flux tube-averaged azimuthal and radial current. These quantities are calculated by integrating each component of $\mathbf{J}_{\perp}$ from (3) along the field line and then dividing by the appropriate grid cell surface area (azimuthal or radial), also integrated along the flux tube. At radial distances greater than the pressure peak (3.5 to 4 R_E), the current flows westward. Inside of this peak the current flows eastward. At the ends of the crescent of high pressure, radial currents complete the loop, flowing away from Earth on the nightside and toward Earth on the dayside. Note that there are essentially no radial currents in the final column because the pressure (and therefore the azimuthal current) is almost completely symmetric.

Because $\mathbf{J}_{\perp}$ from (1) is a curl, its divergence is zero and it therefore does not contribute to $J_{\|}$. Examination of (2) indicates that a FAC is generated when either $P_{\perp}$ or $P_{\|}$ vary along a line of constant magnetic flux density (in the present case,

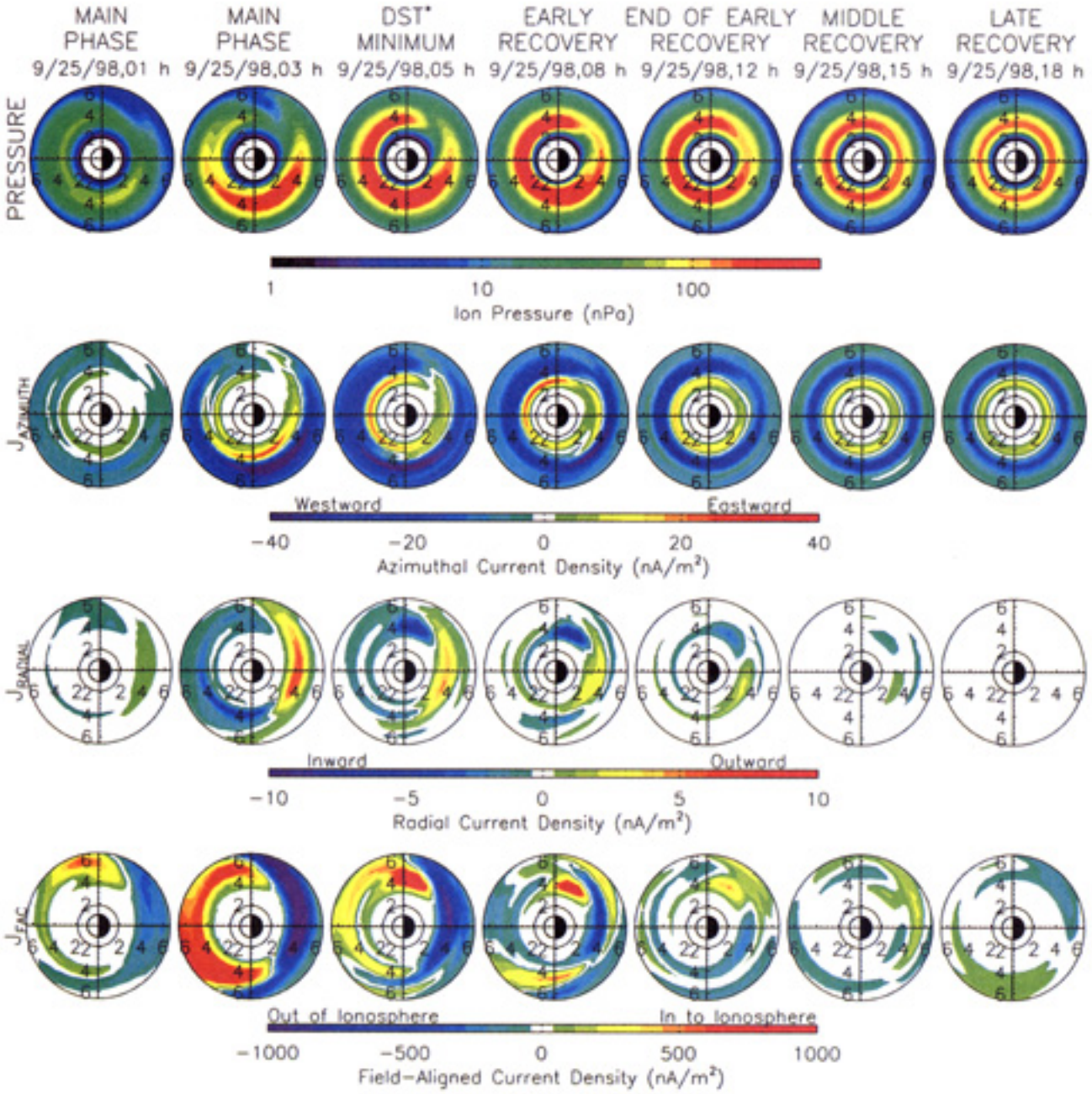

Plate 1. Dial plots of September 25, 1998, storm. The seven columns are at 0100 and 0300 UT (main phase), 0500 UT (modeled *Dst** minimum), 0800 UT (early recovery), 1200 UT (end of early recovery), and 1500 and 1800 UT (late recovery phase). The four rows present field line-averaged values of the energy density, azimuthal current, radial current, and the ionospheric (120 km) value of the field-aligned current. Note that each row has its own colorscale, the first one logarithmic. In each plot the view is looking down from over the North Pole, with noon to the left and distances given in R_E.

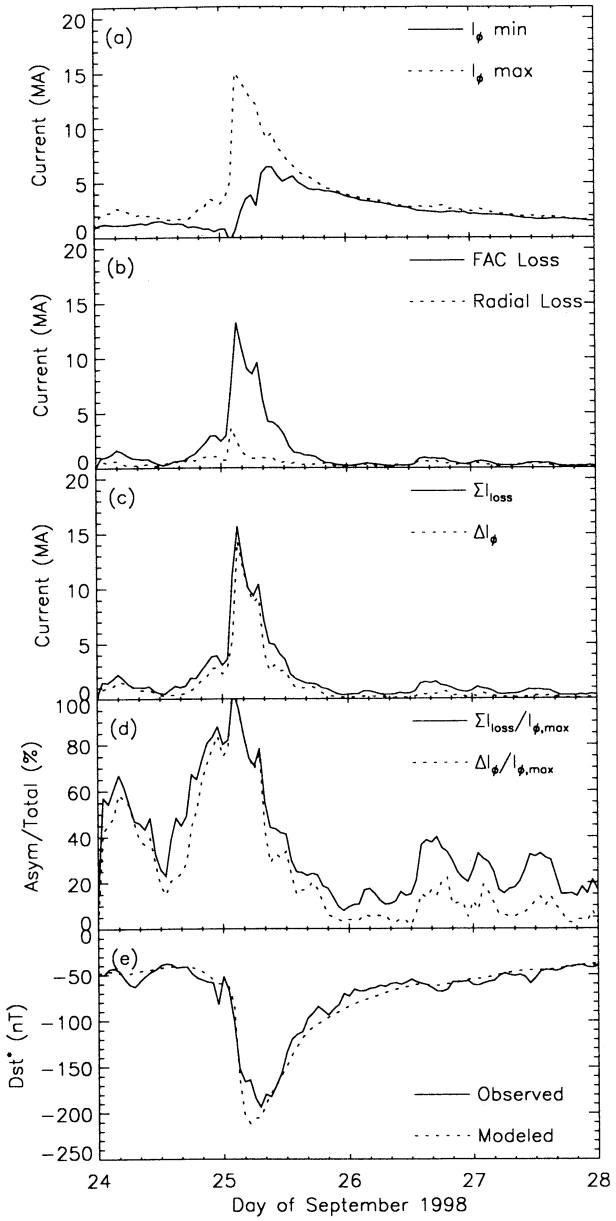

Figure 2. Integrated current quantities for the September 1998 storm. Shown are (a) the maximum and minimum azimuthal current through an LT slice, (b) the total field-aligned current into the ionosphere and the total radial current out of the simulation domain, (c) the partial ring current from subtraction of the values in Figure 2a and also from summation of the values in Figure 2b, (d) the percentage of the total current that is asymmetric, calculated as shown in the legend, and (e) the observed and modeled *Dst** profiles.

along an L shell). Because the ion pressure has a crescent morphology (rather than a torus), it has an azimuthal gradient and thus FACs are generated. In general, downward FACs are generated where the pressure increases with local time and upward FACs are generated where the pressure decreases with local time. This is seen in the last row of Plate 1 where the $J_\parallel$ into (or out of) one ionosphere is shown (ionospheric current density, not a flux tube-averaged value). Note that the values shown are the current densities at 120 km altitude in the northern ionosphere, but they are plotted on an equatorial spatial grid for similarity with the other dial plots in Plate 1. These current densities reach values greater than 1 μA m^{-2}, which, compared with typical stormtime high-latitude FAC densities of a few μA m^{-2}, are approaching very significant levels of current flow through the ionosphere. In addition, they are deposited at subauroral latitudes, where the ionospheric closure currents have the possibility of greatly influencing the low and midlatitude magnetometer stations used to calculate the *Dst* index. Such an effect was found for large substorm current wedges [*Friedrich et al.*, 1999; *Munsami*, 2000] and could happen here, although calculation of this impact is beyond the scope of this paper. However, a qualitative discussion of this impact is given in the next section.

The $J_\parallel$ values in Plate 1 illustrate an interesting phenomenon. Before the storm the FACs have the standard pattern (but very weak) of being out of the ionosphere on the dawnside and into the ionosphere on the duskside. As the plasma pressures and convection strength increase, this pattern is rapidly changed into the storm main phase noon-midnight configuration. This breaks up, weakens, and rotates around throughout the recovery phase (columns 5 and 6) to eventually return to the dawn-dusk region 2 configuration (column 7). What is seen in the sequence of dial plots is that the pattern moves westward through 360° of azimuth, rather than rotating back eastward as the disturbance wanes. The rotation is because the ion pressure enhancement generating these currents gradient-curvature drifts westward through near-Earth space after the ions are captured onto closed trajectories. This occurs simultaneously with the buildup of the standard region 2 Birkeland currents seen in the final column. Column 6 reveals a complicated FAC pattern as the stormtime system rotates and decays while the standard region 2 FAC pattern emerges at the outer edge of the simulation domain. During the rotation the electric field pattern generated by the ionospheric closure of these FACs moves into and out of phase with the region 1 current-generated electric fields. Such phase oscillation will have an influence on the inner magnetospheric plasma, particularly the cold population of the plasmasphere.

The FAC pattern seen in the lower-right dial plot of Plate 1 persists through the remainder of the simulation (another day). While it is slightly offset from midnight, this offset is also present in the prescribed high-latitude-driven convection pattern (the modified McIlwain field [see *Liemohn et al.*, 2001, Figure 5] and thus the basic pattern matches that of the standard quiet time region 2 Birkeland currents.

3.2. Integral Current Characteristics

Plate 1 appears to be highly asymmetric in pressure and azimuthal current during the main phase and early recovery phase of the storm. To obtain a global measure of the asymmetry in the ring current, it is useful to integrate the azimuthal current density over radial distance and latitude at various local times, yielding the total westward current as a function of local time (LT). The symmetric ring current at a particular time would therefore be the LT minimum of this integral value, because it is the current that flows completely around the Earth. The asymmetric portion of the ring current is defined here as the maximum of this integral value minus the minimum value, because this is azimuthal current that does not make it all the way around the Earth. Plotted in Figure 2a are the maximum (symmetric plus asymmetric) and minimum (symmetric only) values of the westward current, and it is clear that there is a strong asymmetry in the ring current during the main phase of the storm. The observed and modeled (from the Dessler-Parker

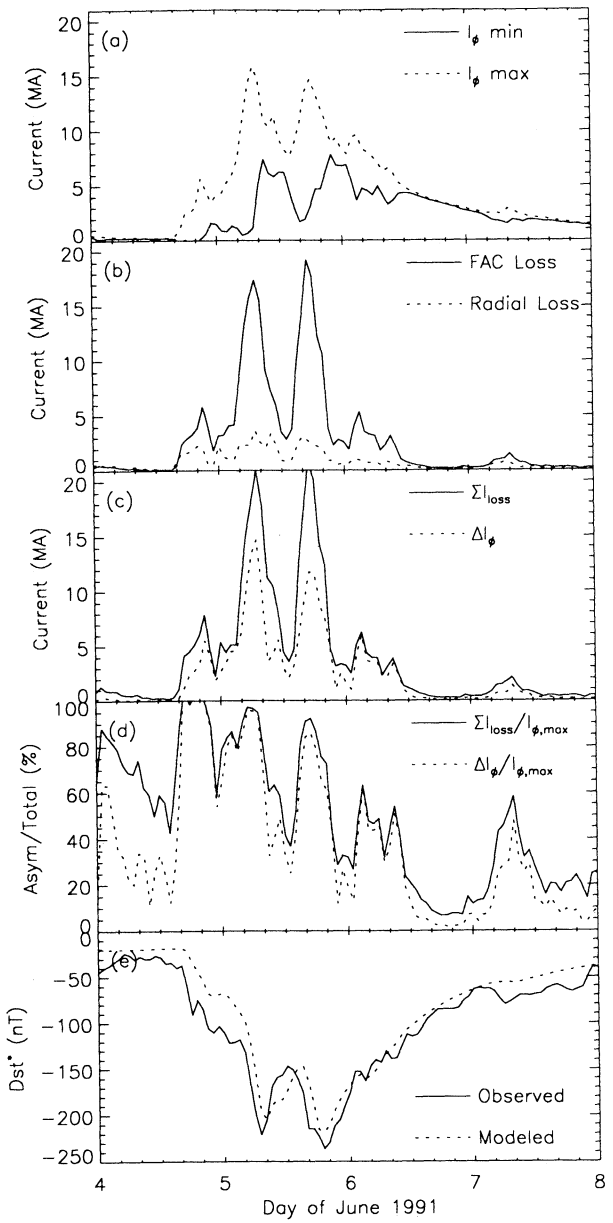

Figure 3. Same as Figure 2, but for the June 1991 storm.

Sckopke relation [*Dessler and Parker*, 1959; *Sckopke*, 1966]) *Dst** is plotted in Figure 2e for timing reference and also to show the overall accuracy of the model results against the observed *Dst** profile. It is interesting to note that the symmetric ring current actually decreases during the early growth phase of the storm (momentarily reaching zero) before rising and reaching a maximum value of 8 MA during the storm recovery.

This current asymmetry must be balanced somehow, though, and there are two ways of removing the excess current from the simulation domain: FACs and radial currents through the outer (and inner) boundary. The integrals for each of these two $\mathbf{J}_\perp$ losses are shown in Figure 2b. The FACs are computed from (6) based on the divergence of $\mathbf{J}_\perp$ inside the simulation domain, while the radial loss is simply $\mathbf{J}_\perp$ from (3) exiting the simulation domain. It should be noted that the $\mathbf{J}_\perp$ sources from these two terms are nearly identical to the loss values at all times, conserving the current through the boundary and through the ionosphere. It is seen in Figure 2b that FAC loss is by far the biggest loss of current. This is significant, because it indicates that the crescent of extra westward current is a partial ring current closed through the ionosphere rather than a magnetotail current closed through the magnetopause. In fact, the radial current loss may also be a FAC into the ionosphere beyond the simulation domain.

Because the partial ring current should match the current losses in the system, it is useful to compare these two quantities. Figure 2c shows the asymmetric ring current intensity calculated two ways: from the subtraction of the maximum and minimum westward current integrals; and from the addition of the FAC and radial current losses (note the addition of the current sources is equal to this). It is seen that the summation value is slightly larger than the subtraction value. This is expected, because the summation value includes partial ring currents that do not pass through the LT of the maximum westward current (that is, some fraction of the asymmetric current flows into and out of the simulation domain without crossing the LT of maximum current). The difference is not large, however, indicating most of the partial ring current is recorded by the subtraction method. Also seen in Figure 2c is the magnitude of the partial ring current (both curves). It peaks sharply up to 15 MA just before the *Dst** minimum. It then decreases during the early recovery phase and remains below 1 MA (for the most part) throughout the late recovery phase of the storm.

This partial ring current during the main phase of the storm is much larger than the symmetric ring current at that time. The percentage of partial ring current (partial over maximum westward current) is shown in Figure 2d. It can be seen that this quantity reaches 100% just before the *Dst** minimum. It declines throughout the recovery, but not as fast as the partial ring current does because the symmetric ring current is also degrading. Late in the storm sequence the percentage is usually below 20%, with occasional excursions above this during mild injections from the tail.

To show the generality of this result, Figures 3, 4, and 5 show analogous results for the three other storms mentioned above. In all cases, the partial ring current is dominant during the main phase and early recovery of the storm, with intensities typically an order of magnitude larger than the prestorm symmetric ring current. The symmetric ring current grows during the early recovery of the storm as the convection strength weakens, and then starts declining in the late recovery phase as charge exchange becomes the dominant ring current loss. Note that these storms have very different modeled *Dst** minima, ranging from -80 to -240 nT, the solar cycle phase is quite different between them, and the solar wind conditions were distinctly different in each case. The main similarity between them is that all four storms are driven by ICMEs and have two-phase decay recoveries. This disparity of storm conditions yet similarity in partial ring current dominance lends support to the claim that this is the case for these types of storms in general.

4. Comparison With Observations

It is useful to compare these current densities with observations of the inner magnetospheric current density during disturbed conditions. For example, *Lui et al.* [1987] showed current densities in the afternoon sector during two magnetic storms. Figure 6 shows a comparison of their observations against model results. Shown here are the observationally

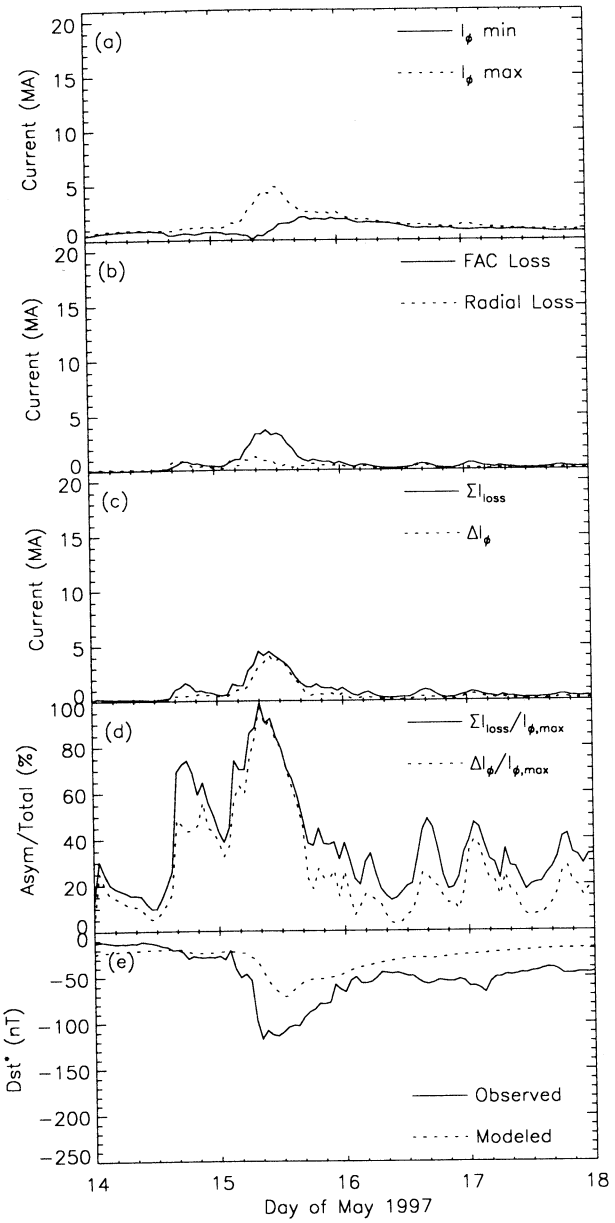

Figure 4. Same as Figure 2, but for the May 1997 storm.

derived current densities from the main phase of a moderate magnetic storm (September 4, 1984) together with results from the main phase of the September 1998 storm along a similar spatial trajectory through the inner magnetosphere (near 1400 LT at L=7 to 1800 LT at L=2). Figure 6a shows the total azimuthal current from the observations and from the model. The profiles have similar shapes and magnitudes. Differences are to be expected because they are from different storms, but both are September storms near solar cycle minimum. Another source of difference is that the observational values are not purely azimuthally flowing currents because the satellite moved in local time, thus measuring a mixture of the strong azimuthal currents and the weaker radial currents. Figures 6b and 6c show the contributions to this current density from the two terms on the right-hand side of (3), the pressure gradient term and the anisotropy-curvature term, respectively. It is seen that the model results are reasonably close to the observational values, particularly with respect to the overall shape of these radial profiles. A comparison of Figures 6b and 6c show that the pressure gradient term is indeed much larger than the other term in the calculation of the perpendicular current density (moreso in the model results than in the measurement-derived currents).

Comparisons with statistical compilations of field-aligned current densities show similar agreement with the model results [e.g., *Iijima and Potemra*, 1976; *Zanetti et al.*, 1984; *Bythrow et al.*, 1984; *Iijima et al.*, 1990; *Weimer*, 1999]. For instance, both *Zanetti et al.* [1984] and *Weimer* [1999] showed nonsubstorm FAC patterns with region 2 currents peaking near 65° invariant latitude (standard dawn-dusk pattern of *Iijima and Potemra* [1976]) with an amplitude of a few tenths of a μA m^{-2} (all interplanetary magnetic field (IMF) clock angles). Compare this with the FAC pattern values of the late recovery phase of the storm shown in Plate 1. Values of a few tenths of μA m^{-2} are shown, with the standard dawn-dusk con-

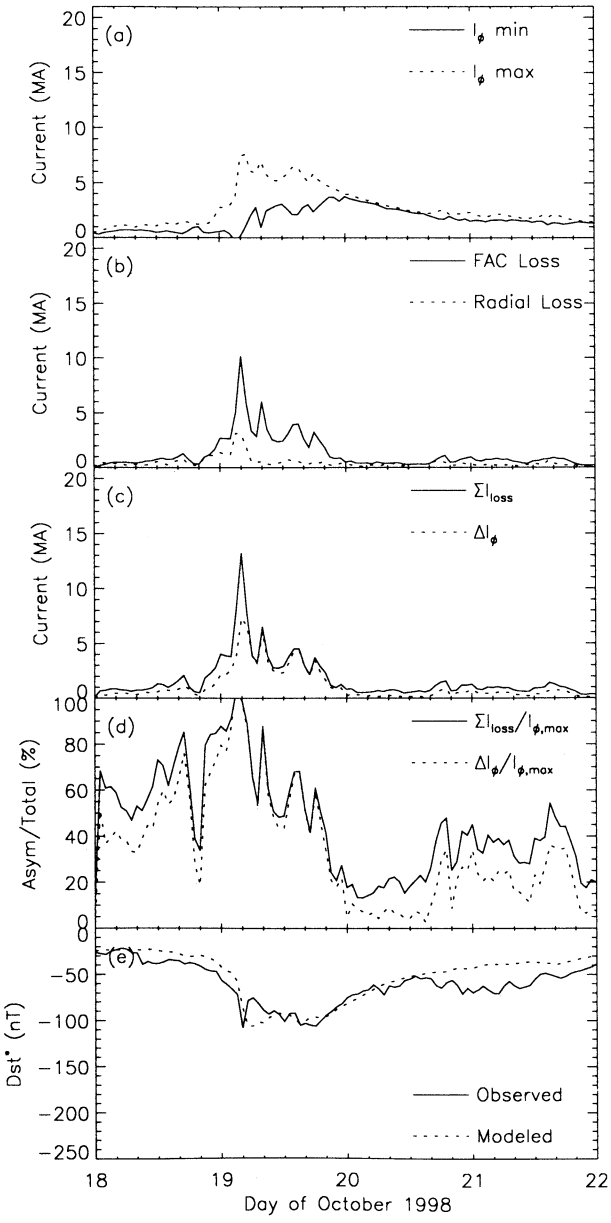

Figure 5. Same as Figure 2, but for the October 1998 storm.

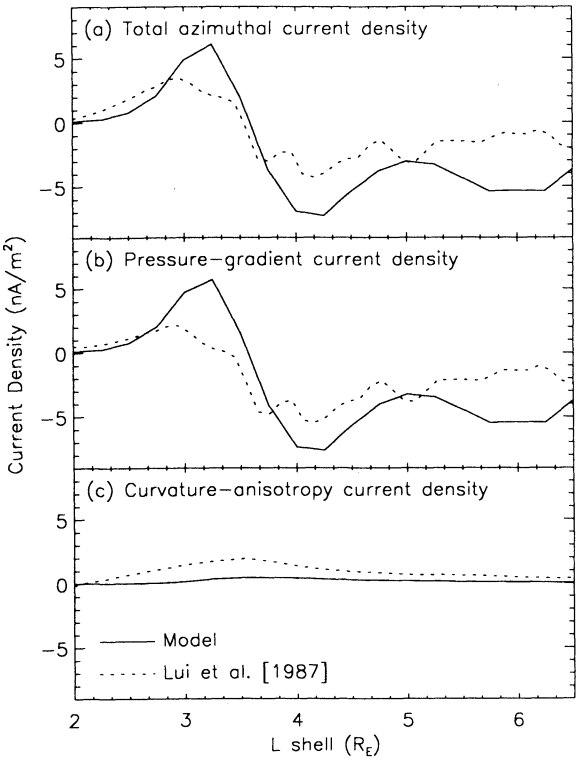

Figure 6. Comparison between modeled and observed azimuthal currents (positive eastward) in the afternoon sector during the main phase of a geomagnetic storm. Shown are (a) total azimuthal current, (b) current from the pressure gradient term in (3), and (c) current from the magnetic curvature (and pressure anisotropy) term in (3). The observed current densities are from *Lui et al.* [1987, Figure 5], during the growth phase of a storm on September 4, 1984. The model results are from 0000 UT on September 25, 1998, for spatial locations matching the trajectory of the satellite.

figuration. *Bythrow et al.* [1984] showed that during periods of strongly southward IMF (-6 nT≥$B_{z,IMF}$≥-11 nT), this pattern moves equatorward, peaking closer to 60° invariant latitude with significantly larger current densities. Similarly, *Weimer* [1999] showed that substorm-epoch FAC patterns move a bit equatorward, rotate westward, and essentially double in intensity (close to 0.5 μA m^{-2}). During storm periods, this pattern is expected to continue to intensify and move equatorward and westward, just as predicted by the model results discussed above. It should be remembered that the simulation domain of the model calculations shown above is within geosynchronous orbit (roughly 67° invariant latitude), so only part of the region 2 Birkeland currents are reproduced in the model results.

Chun and Russell [1997, 2000] statistically compiled magnetic perturbation data from several inner magnetospheric satellites. They determined that there is a large occurrence rate of FACs in the premidnight region inside of geosynchronous orbit (down to R=3 R_E, the extent of their study) during active geomagnetic periods. However, during low-activity periods, this feature disappears and the median region 2 FAC location moves out near geosynchronous orbit (R=6-8 R_E), consistent with the well-known *Iijima and Potemra* [1976] ionospheric FAC pattern. Such a morphology and evolution of the FAC pattern in the inner magnetosphere is clearly seen in the model results.

The results are also consistent with plasma pressure measurements in the inner magnetosphere and the generation of region 2 Birkeland currents from these observations. The plasma sheet is almost always seen across the nightside local time sector at geosynchronous orbit, with excursions away from this norm mostly during very disturbed times when the satellites enter the lobe [*McComas et al.*, 1993]. Furthermore, inner magnetospheric satellite observations consistently show an increasing plasma pressure in to L=3 or 4, even for quiet times [e.g., *Lui and Hamilton*, 1992; *Lui et al.*, 1994]. Such an ion pressure profile requires an alternative FAC generation scenario in order to explain the location of the region 2 Birkeland currents (see *Mauk and Zanetti* [1987] for a detailed discussion of this). *Lui et al.* [1994] proposed that a pressure gradient directed more toward the midnight meridian than the magnetic field gradient (yet both pointing toward the Earth) is a configuration suitable to producing region 2 currents of the proper sense when the pressure increases toward the Earth. This is exactly the configuration that exists in the model results shown above (late recovery and quiet times), with an enhancement of pressure near midnight relative to the nightside flanks. This enhancement is from a pileup of ions as the corotation, convection, and gradient-curvature components of the perpendicular drift create a stagnation point near this location for certain energies. Figure 7 shows the Alfvén boundaries for three ion energies (0, 3, and 12 keV at R=6.6 R_E) for typical low geomagnetic activity values (using a modified McIlwain convection field, as used in the simulation results). These energies span the range of typical nightside plasma sheet temperatures observed at geosynchronous orbit, which are usually from 5 to 8 keV [e.g., *Borovsky et al.*, 1998]. The stagnation point of the boundary rotates from slightly postdusk for zero-energy ions through midnight into the predawn sector for high-energy ions. The ion population is enhanced on either side of the Alfvén boundary because these are typically the slowest-flowing drift trajectories through the inner magnetosphere (zero flow at the stagnation point). In addition, loss processes such as Coulomb collisions and charge exchange reduce the ion fluxes as the particles convect through the inner magnetosphere. These factors lead to a hot ion pressure morphology that fits well with the observations, and produces the proper sense of region 2 currents in the inner magnetosphere during quiet times.

The results presented above are also consistent with ground-based observations. *Clauer et al.* [1983] found that ASYM, the dawn-dusk asymmetry in the northward magnetic field perturbation in midlatitude ground-based magnetometer measurements, is correlated with the solar wind motional electric field E_y with a 3 hour time lag, while ASYM was not particularly well correlated with the *AL* index of auroral activity. This indicates that ASYM is generated by the injection of plasma sheet ions in close to the Earth (a trait of strong E_y), as is the case for the storms studied here [*Liemohn et al.*, 2001; Kozyra et al., submitted manuscript, 2001]. *Iyemori* [1990], also analyzing stormtime midlatitude magnetometer data, found, on average, downward FACs in the late morning and upward FACs in the evening to early morning. During storm main phases, however, the downward FAC peak was located in the afternoon, and shifted to the morning sector as storms progress. This is precisely the FAC evolution and morphology presented in Plate 1.

All of this leads to the conclusion that the model fairly accurately determines the currents in the inner magnetosphere

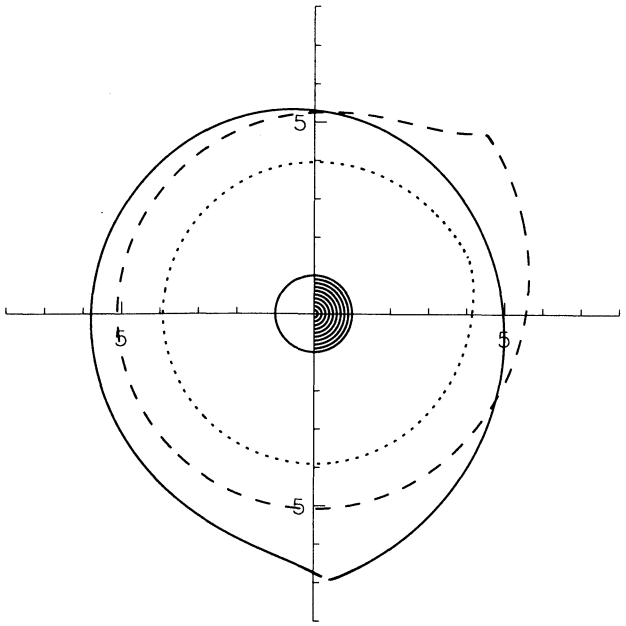

Figure 7. Alfvén boundaries asusming a modified McIlwain convection electric field for typical low-activity levels (Kp=2, cross polar cap potential of 40 kV, and magnetospheric width of 30 R_E). Three boundaries are shown corresponding to ion energies of 0 keV (solid line), 3 keV (dotted line), and 12 keV (dashed line) at geosynchronous orbit (magnetic moments of 0, 28, and 111 eV nT^{-1}, respectively). The view is looking down from over the North Pole, with noon to the left and distances given in R_E.

during geomagnetic storms. This is true even though the model uses a static dipole magnetic field and an electric field description is an imposed analytical formulation driven by solar wind and geomagnetic activity conditions (resulting in a temporally and spatially varying convection pattern). Self-consistent magnetic and electric field descriptions would certainly improve the data-theory comparisons, but the closeness of the simulation results to the observations lends support to the claim that these nonlinear effects are not large. Furthermore, it is possible to use these model results to extrapolate single-point or multipoint observations of the current into a global picture of the magnetospheric currents in near-Earth space. Of course, this is already happening, to some degree, not only in the model results shown here (extrapolating geosynchronous observations into a solution throughout the inner magnetosphere) but also with data assimilation inside of the calculational domain of a transport model [*Garner et al.*, 1999].

5. Discussion

The results above show that numerical calculations of the stormtime energetic ion distributions in the inner magnetosphere yield a highly asymmetric ring current during the main phase which eventually transitions into a highly symmetric ring current during the late recovery phase. In addition, these results are consistent with ground-based, ionospheric, and inner magnetospheric observations of storm periods, supporting the claim that these results are generalizable to most (or all) ICME-driven, two-phase decay storms. Let us now examine in more detail some of the features of these results.

It is interesting that three of the four storms presented had at least one instance of a ring current that was 100% asymmetric (and the other one came very close). This always occurred during the main phase of the storm. During these instances, the minimum net westward current is zero or negative. This is a bit misleading, because it does not mean there is no westward current at some dawnside LT. Rather it means that the eastward current is equal to or exceeds the westward current at this LT, making the integral over the meridional plane slice less than zero. This is partly caused by the numerical resolution of the results from the kinetic ion transport code. Another, more important, reason is an increased eastward current on the dawnside created by the morphology of the partial ring current at this time. That is, the pressure peak moves to large L values in the predawn sector during enhanced particle injection intervals. Consequently, the eastward-westward pair of azimuthal currents is moved outward during these times, so much so that there is a particular LT interval where the eastward current dominates (the westward current is beyond the simulation domain). This is seen in Plate 1 in the two left-most columns, not only in the predawn sector at large radial distances (beyond 5 R_E) as a tail in the energy density plots but also in the corresponding azimuthal current density plots. As seen there, westward current exists at all local times, it is just weaker than the eastward current at some instances during the injection phase of the storm. Regardless, the symmetric component of the ring current is very small (if not actually zero) at these times, and the asymmetric component dominates throughout this phase of the storm.

The closure of the asymmetric $\mathbf{J}_\perp$ through FACs (rather than the magnetopause) is necessary because current must be conserved everywhere. Because $\mathbf{I}_\perp$ defines the current in two spatial coordinates, any divergence of this current must be balanced by a current in the third spatial coordinate (that is, along the geomagnetic field lines). Although other theoretical studies have assumed that cross-field magnetospheric currents inside of geosynchronous orbit close through the magnetopause [e.g., *Alexeev et al.*, 1996], the present calculations indicate most of the asymmetric $\mathbf{J}_\perp$ near the Earth closes through the ionosphere. This has been confirmed by analyses of the east-west magnetic perturbation at low-latitude ground-based magnetometer stations, which show signatures consistent with the ionospheric closure currents presented here in Plate 1 [*Iyemori*, 1990; C. R. Clauer et al., manuscript in preparation, 2001].

The results presented above all used the same model of the convection electric field, yet it is known that the choice of this description is critical to the nature of the flow of the hot ions through the inner magnetosphere [cf., *Korth et al.*, 1999; *Jordanova et al.*, 1999]. Therefore it is useful to show a comparison of the stormtime ring current strength from at least one other convection field description. Figure 8 shows such a comparison for the September 1998 storm for several components of the azimuthal current from the modified McIlwain (MM) field (used throughout this study) with results using an MBI-driven Volland-Stern (VS) electric field description [*Volland*, 1973; *Stern*, 1975]. It is seen that the VS model predicts less symmetric ring current during the recovery phase of the storm, but the amount of asymmetric ring current is very similar between the two descriptions. This lower level of symmetric ring current is because the morphology of the VS convection pattern is such that flow-through is stronger relative to the MM model. Therefore less of the ions are trapped onto

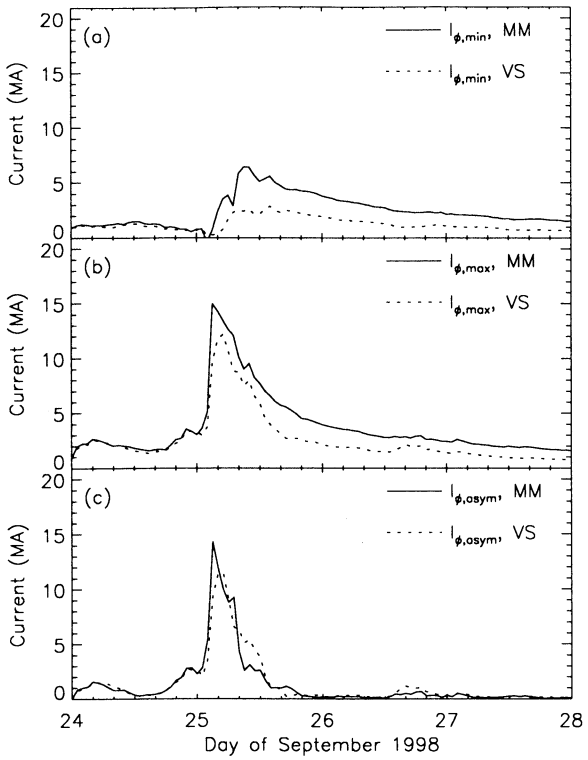

Figure 8. Comparison of azimuthal current values for the September 1998 storm from the modified McIlwain (MM) and Volland-Stern (VS) convection electric field descriptions. Shown are (a) the minimum azimuthal current through an LT slice, (b) the maximum azimuthal current through an LT slice, and (c) the asymmetric azimuthal ring current found from the subtraction of the minimum from the maximum values.

closed trajectories during the recovery phase. The similarity in the asymmetric ring current component, however, indicates that the two electric field descriptions yield very similar particle inflow rates.

The results of this study should also be compared with the inner magnetospheric magnetic field calculations of *Tsyganenko* [2000]. In that study, the symmetric and asymmetric ring currents were assumed to have azimuthal currents of less than 1 MA each. In the present results, the two ring current components also reach values of less than 1 MA, but only during quiet times, and the stormtime conditions are much different. The asymmetric current component can reach 15-20 MA during the main phase of a storm and the symmetric portion can rise up to several MA during the recovery phase. These differences are expected, though, because *Tsyganenko* [2000] assumed quiet time ring current ion distributions (those of *Lui and Hamilton* [1992]). Therefore the results from that study and this one are not at odds but are actually quite consistent. In fact, the model development of that study can be applied to the current density distributions obtained in this study.

Because of the rich history of the RCM in modeling the electrodynamics of the inner magnetosphere, it is worthwhile to compare the present results against results from that model. A direct comparison against the idealized case studies of *Spiro et al.* [1988] is not appropriate because these were hour-long substorm injections, while this study is examining day-long storm conditions. The general trend is very similar between the two studies, however, and the results presented here appear to be dramatically perturbed cases compared to their isolated substorm simulations. A direct comparison can be made, however, with the study of *Garner* [2000], who used the RCM to examine one of the storms included in this study (June 1991). They achieved good data comparison for the calculated electric fields, but less so for the calculated ion fluxes. The opposite is essentially true for our model, with its prescribed analytical electric field formulation but with good data-theory comparisons of ion flux [Kozyra et al., submitted manuscript, 2001]. The resulting electric fields generated by the FACs presented in this study are morphologically similar to those of the RCM and also are quite consistent with observed electric fields [*Ridley and Liemohn*, 2001]. The two models should not give exactly the same results because the computational schemes and boundary conditions are quite different. While the electric field is self-consistently calculated in the RCM, the model used for this study has its own advantages, such as inclusion of realistic loss functions and a highly resolved velocity space distribution. Self-consistency of the electric field (and eventually the magnetic field) calculation is presently being incorporated. In addition, recent studies have used the RCM in "ring current mode," showing stormtime injection of plasma sheet particles deep into the inner magnetosphere [*Fok et al.*, 2001; S. Sazykin et al., unpublished study, 2001]. It is clear that plasma transport models of the near-Earth space region are converging on comprehensive calculational techniques that accurately reproduce the observations.

6. Conclusions

The main conclusions from this study are as follows.

1. Hot ion transport models are able to reproduce the observed morphology and intensity of the currents in the inner magnetosphere, allowing for the examination of the three-dimensional current system for specific events and for the extrapolation of observed values of the current or ion flux throughout near-Earth space.

2. The perpendicular current in the inner magnetosphere is largely asymmetric during the main phase and early recovery phase of ICME-driven, two-phase decay geomagnetic storms. As the convection strength decreases, the particles are trapped on closed drift paths and the current pattern transforms into the classic symmetric ring current.

3. For large storms (Dst_{min}<-200 nT), the asymmetric current can reach 20 MA, while the symmetric current can reach up to 8 MA (note that both do not peak at the same time). In general, the peak asymmetric current is 2-3 times larger than the peak symmetric current during any particular event.

4. Most of this asymmetric current closes through Birkeland currents into the mid-latitude ionosphere (rather than through magnetopause currents), and thus it should be classified as a partial ring current rather than a near-Earth tail current.

5. The stormtime FAC pattern rotates westward completely around the Earth as the captured ions gradient-curvature drift on closed trajectories. This occurs while the quiet time region 2 FAC pattern is reforming in the open trajectory region just beyond the hot ion Alfvén boundaries. Therefore during the recovery phase of the storm a complicated pattern of time-varying FACs appears that will generate a highly structured electric field that is not necessarily in phase with the region 1 current-generated electric field pattern.

6. During storm late recovery and quiet times the model reproduces a pressure maximum near local midnight, consistent with the region 2 current generation mechanism described by *Lui et al.* [1994] for an earthward pointing pressure gradient.

This analysis raises many questions that should be addressed. For instance, the FACs will create an electric potential difference in the ionosphere, particularly on the midlatitude nightside where the conductivity is low, which will have consequences for ionospheric and magnetospheric plasma flows [e.g., *Fejer et al.*, 1990; *Yeh et al.*, 1991]. It also raises the issue of the stormtime asymmetry of the magnetic perturbation, and the contributions to this asymmetry from $\mathbf{J}_\perp$ and from the closure current segments. While a number of studies have examined this with idealized ring current constructions [e.g., *Akasofu and Chapman*, 1964; *Crooker and Siscoe*, 1974, 1981; *Takahashi et al.*, 1991], a rigorous and accurate calculation for the stormtime ring current has not yet been performed. Yet another concern is the validity of the DPS relation when the ring current is highly asymmetric. These issues are presently being explored.

Acknowledgments. This work was supported by NASA grant NAG5-4771 and NSF contracts ATM-9711381, ATM-9800830, and ATM-9801941. The authors would also like to thank all of the data providers that make the ring current simulations possible, especially M. F. Thomsen and J. E. Borovsky at Los Alamos National Laboratory, the Wind and ACE particle and field instrument teams, the Air Force Research Laboratory at Hanscom AFB, and the Kyoto World Data Center. The authors would like to thank both referees for useful comments regarding this manuscript.

Janet G. Luhmann thanks Nikolai Tsyganenko and another referee for their assistance in evaluating this paper.

References

Akasofu, S.-I., and S. Chapman, On the asymmetric development of magnetic storm fields in low and middle latitudes, *Planet. Space Sci., 12*, 607, 1964.

Alexeev, I. I., E. S. Belenkaya, V. V. Kalegaev, Y. I. Feldstein, and A. Grafe, Magnetic storms and magnetotail currents, *J. Geophys. Res., 101*, 7737, 1996.

Birmingham, T. J., Birkeland currents in an anisotropic, magnetostatic plasma, *J. Geophys. Res., 97*, 3907, 1992.

Borovsky, J. E., M. F. Thomsen, and R. C. Elphic, The driving of the plasma sheet by the solar wind, *J. Geophys. Res., 103*, 17,617, 1998.

Bythrow, P. F., T. A. Potemra, and L. J. Zanetti, Variation of the auroral Birkeland current pattern associated with the north-south component of the IMF, in *Magnetospheric Currents, Geophys. Monogr. Ser.*, vol. 28, edited by T. A. Potemra, p. 131, AGU, Washington, D. C., 1984.

Chen, C.-K., R. A. Wolf, M. Harel, and J. L. Karty, Theoretical magnetograms based on quantitative simulation of a magnetospheric substorm, *J. Geophys. Res., 87*, 6137, 1982.

Chun, F. K., and C. T. Russell, Field-aligned currents in the inner magnetosphere: Control by geomagnetic activity, *J. Geophys. Res., 102*, 2261, 1997.

Chun, F. K., and C. T. Russell, Statistical characteristics of field-aligned currents in the Earth's inner magnetosphere, in *Magnetospheric Current Systems, Geophys. Monogr. Ser.*, vol. 118, edited by S.-I. Ohtani, R. Fujii, M. Hesse, and R. L. Lysak, p. 237, AGU, Washington, D. C., 2000.

Clauer, C. R., R. L. McPherron, and C. Searls, Solar wind control of the low-latitude asymmetric magnetic disturbance field*J. Geophys. Res., 88*, 2123, 1983.

Crooker, N. U., and G. L. Siscoe, Model geomagnetic disturbance from asymmetric ring current particles, *J. Geophys. Res., 79*, 589, 1974.

Crooker, N. U., and G. L. Siscoe, Birkeland currents as the cause of the low-latitude asymmetric disturbance field, *J. Geophys. Res., 86*, 11,201, 1981.

Daglis, I. A., R. M. Thorne, W. Baumjohann, and S. Orsini, The terrestrial ring current: Origin, formation and decay, *Rev. Geophys., 37*, 407, 1999.

Dessler, A. J., and E. N. Parker, Hydromagnetic theory of geomagnetic storms, *J. Geophys. Res., 64*, 2239, 1959.

Ebihara, Y., and M. Ejiri, Modeling of solar wind control of the ring current buildup: A case study of the magnetic storms in April 1997, *Geophys. Res. Lett., 25*, 3751, 1998.

Ebihara, Y., and M. Ejiri, Simulation study on fundamental properties of the storm-time ring current, *J. Geophys. Res., 105*, 15,843, 2000.

Fejer, B. G., and L. Scherliess, Empirical models of storm time equatorial zonal electric fields, *J. Geophys. Res., 102*, 24,047, 1997.

Fejer, B. G., R. W. Spiro, R. A. Wolf, and J. C. Foster, Latitudinal variation of perturbation electric fields during magnetically disturbed periods: 1986 SUNDIAL observations and model results, *Ann. Geophys., 8*, 441, 1990.

Fok, M.-C., J. U. Kozyra, A. F. Nagy, C. E. Rasmussen, and G. V. Khazanov, A decay model of equatorial ring current and the associated aeronomical consequences, *J. Geophys. Res., 98*, 19,381, 1993.

Fok, M.-C., R. A. Wolf, R. W. Spiro, and T. E. Moore, Comprehensive computational model of Earth's ring current, *J. Geophys. Res., 106*, 8417, 2001.

Friedrich, E., G. Rostoker, and M. G. Connors, Influence of the substorm current wedge on the *Dst* index, *J. Geophys. Res., 104*, 4567, 1999.

Garner, T. W., A case study of the June 4-5, 1991, magnetic storm using the Rice Convection Model, Ph.D. thesis, Rice Univ., Houston, Tex., 2000.

Garner, T. W., R. A. Wolf, R. W. Spiro, and M. F. Thomsen, First attempt at assimilating data to constrain a magnetospheric model, *J. Geophys. Res., 104*, 25,145, 1999.

Grafe, A., Are our ideas about *Dst* correct?, *Ann. Geophys., 17*, 1, 1999.

Greenspan, M. E., and D. C. Hamilton, A test of the Dessler-Parker-Sckopke relation during magnetic storms, *J. Geophys. Res., 105*, 5419, 2000.

Hamilton, D. C., G. Gloeckler, F. M. Ipavich, W. Studemann, B. Wilkey, and G. Kremser, Ring current development during the great geomagnetic storm of February 1986, *J. Geophys. Res., 93*, 14343, 1988.

Harel, M., R. A. Wolf, P. H. Reiff, R. W. Spiro, W. J. Burke, F. J. Rich, and M. Smiddy, Quantitative simulation of a magnetospheric substorm, 1, Model logic and overview, *J. Geophys. Res., 86*, 2217, 1981.

Iijima, T., and T. A. Potemra, The amplitude distribution of field-aligned currents at northern latitudes observed by TRIAD, *J. Geophys. Res., 81*, 2165, 1976.

Iijima, T., T. A. Potemra, and L. J. Zanetti, Large-scale characteristics of magnetospheric equatorial currents, *J. Geophys. Res., 95*, 991, 1990.

Iyemori, T., Storm-time magnetospheric currents inferred from mid-latitude geomagnetic field variations, *J. Geomagn. Geoelectr., 42*, 1249, 1990.

Jaggi, R. K., and R. A. Wolf, Self-consistent calculation of the motion of a sheet of ions in the magnetosphere, *J. Geophys. Res., 78*, 2842, 1973.

Jordanova, V. K., L. M. Kistler, J. U. Kozyra, G. V. Khazanov, and A. F. Nagy, Collisional losses of ring current ions, *J. Geophys. Res., 101*, 111, 1996.

Jordanova, V. K., R. B. Torbert, R. M. Thorne, H. L. Collin, J. L. Roeder, and J. C. Foster, Ring current activity during the early $Bz<0$ phase of the January 1997 magnetic cloud, *J. Geophys. Res., 104*, 24,895, 1999.

Korth, H., M. F. Thomsen, J. E. Borovsky, and D. J. McComas, Plasma sheet access to geosynchronous orbit, *J. Geophys. Res., 104*, 25,047, 1999.

Liemohn, M. W., J. U. Kozyra, V. K. Jordanova, G. V. Khazanov, M. F. Thomsen, and T. E. Cayton, Analysis of early phase ring current recovery mechanisms during geomagnetic storms, *Geophys. Res. Lett., 26*, 2845, 1999.

Liemohn, M. W., J. U. Kozyra, M. F. Thomsen, J. L. Roeder, G. Lu, J. E. Borovsky, and T. E. Cayton, The dominant role of the asymmetric ring current in producing the stormtime *Dst**, *J. Geophys. Res., 106*, 10,883, 2001.

Lui, A. T. Y., and D. C. Hamilton, Radial profiles of quiet time magnetospheric parameters, *J. Geophys. Res., 97*, 19,325, 1992.

Lui, A. T. Y., R. W. McEntire, and S. M. Krimigis, Evolution of the ring current during two geomagnetic storms, *J. Geophys. Res., 92*, 7459, 1987.

Lui, A. T. Y., H. E. Spence, and D. P. Stern, Empirical modeling of the quiet time nightside magnetosphere, *J. Geophys. Res., 99*, 151, 1994.

Mauk, B. H., and L. J. Zanetti, Magnetospheric electric fields and currents, *Rev. Geophys., 25*, 541, 1987.

McComas, D. J., S. J. Bame, B. L. Barraclough, J. R. Donart, R. C. Elphic, J. T. Gosling, M. B. Moldwin, K. R. Moore, and M. F. Thomsen, Magnetospheric plasma analyzer: Initial three-spacecraft observations from geosynchronous orbit, *J. Geophys. Res., 98*, 13,453, 1993.

McIlwain, C. E., A *Kp* dependent equatorial electric field model, *Adv. Space Res., 6* (3), 187, 1986.

Munsami, V., Determination of the effects of substorms on the storm-time ring current using neural networks, *J. Geophys. Res., 105*, 27,833, 2000.

Parker, E. N., Newtonian development of the dynamical properties of ionized gases of low density, *Phys. Rev., 107*, 924, 1957.

Ridley, A. J., and M. W. Liemohn, A model-derived description of the penetration electric field, *J. Geophys. Res.*, in press, 2001.

Sckopke, N., A general relation between the energy of trapped particles and the disturbance field near the Earth, *J. Geophys. Res., 71*, 3125, 1966.

Spiro, R. W., R. A. Wolf, and B. G. Fejer, Penetration of high-latitude-electric-field effects to low latitudes during SUNDIAL 1984, *Ann. Geophys., 6*, 39, 1988.

Stern, D. P., The motion of a proton in the equatorial magnetosphere, *J. Geophys. Res., 80*, 595, 1975.

Takahashi, S., M. Takeda, and Y. Yamada, Simulation of storm-time partial ring current system and the dawn-dusk asymmetry of geomagnetic variation, *Planet. Space Sci., 39*, 821, 1991.

Terada, N., T. Iyemori, M. Nosé, T. Nagai, H. Matsumoto, and T. Goka, Storm-time magnetic field variations observed by the ETS-VI satellite, *Earth Planets Space, 50*, 853, 1998.

Tsyganenko, N., Modeling the inner magnetosphere: The asymmetric ring current and region 2 Birkeland currents revisited, *J. Geophys. Res., 105*, 27,739, 2000.

Vasyliunas, V. M., Mathematical models of magnetospheric convection and its coupling to the ionosphere, in *Particles and Fields in the Magnetosphere*, edited by B. M. McCormac, p. 60, D. Riedel, Norwell, Mass., 1970.

Volland, H. A semiempirical model of large-scale magnetospheric electric fields, *J. Geophys. Res., 78*, 171, 1973.

Weimer, D. R., Substorm influence on the ionosphere electric potentials and currents, *J. Geophys. Res., 104*, 185, 1999.

Yeh, H.-C., J. C. Foster, F. J. Rich, and W. Swinder, Storm time electric field penetration observed at mid-latitude, *J. Geophys. Res., 96*, 5707, 1991.

Zanetti, L. J., W. Baumjohann, T. A. Potemra, and P. F. Bythrow, Three-dimensional Birkeland-ionospheric current system, determined from Magsat, in *Magnetospheric Currents, Geophys. Monogr. Ser.*, vol. 28, edited by T. A. Potemra, p. 123, AGU, Washington, D. C., 1984.

C. R. Clauer, J. U. Kozyra, M. W. Liemohn, and A. J. Ridley, Space Physics Research Laboratory, University of Michigan, 2455 HAyward Street, Ann Arbor, MI 48109-2143, USA. (liemohn@umich.edu)

(Received February 14, 2001; revised July 30, 2001;
accepted July 30, 2001.)